Numerical Investigation of Burst Wave Lithotripsy and Synthesis of Shock and Burst Waves

Mahdi Moghimnezhad, Azadeh Shahidian*

Department of Mechanical Engineering, K. N. Toosi University of Technology, Tehran, Iran

ABSTRACT: The burst wave lithotripsy is a cutting-edge non-invasive treatment for kidney stones. Due to their paramount importance, efforts for elevating the effectiveness of non-invasive treatment have been always amongst researchers' top priorities. The purpose of the current study is numerically investigating the details of exerted stress and the effects of some parameters such as pressure amplitude, frequency and stone's material for burst wave lithotripsy, and feasibility study of the synthesis of shock and burst waves. In addition, thermal side effects are investigated on surrounding tissues for both methods. The COMSOL Multiphysics based on finite element method is utilized to couple and solve the governing non-linear equations of acoustic wave propagation, the elasticity of structure and biological heat transfer. The results for BWL show that increases in pressure amplitude do not change the distribution of von Mises stress. In addition, increasing frequency leads to a reduction of the focal region, which reduced damages to adjacent tissues. The result for the synthesis of the shock wave and burst wave shows that due to the return of the shock wave from the stone, a wall of compressive wave is created in the front of the stone, and it prevents the burst wave to reach the stone. Therefore, the location of the maximum pressure changes and side effects on the kidney tissue increases.

1- INTRODUCTION

Ultrasonic waves have a variety of applications in medicine, such as drug delivery, lithotripsy, hyperthermia and diagnostic imaging. Ultrasonic imaging helps to achieve more information in a non-invasive diagnosis process. In addition, therapeutic applications of ultrasound develop the treatment efficiency and decrease the side effects. For instance, Aayani et al. [1] numerically studied acoustic streaming for drug delivery through the blood flow. Yousefi et al. [2] applied an acoustic wave for aerosol delivery to a human lung. López-Haro et al. [3] modeled the acoustic absorption in biological tissues for hyperthermia purposes. Zohdi and Krone [4] provided a numerical model for estimating the acoustics-induced temperature profile within a multiphase tissue.

Kidney stone disease is a common problem worldwide with a prevalence of approximately 10-12% of men and 5-6% of women in Western countries [5]. Several factors such as genetic, nutrition, geographic and socioeconomic have influences on this disease [6]. There are different types of minerals form urinary stones, and Calcium Oxalate is the most common stone component [7]. There are two main approaches for ultrasonic lithotripsy, Shock Wave Lithotripsy (SWL) and Burst Wave Lithotripsy (BWL). The SWL method typically uses single-cycle focused pulses at a low frequency and high peak pressures. In contrast, the BWL applies short bursts of focused, sinusoidal ultrasonic pulses [8]. SWL as a popular treatment is the only non-invasive lithotripsy in clinical application since 1980 [9, 10]. BWL is a new technology as a potentially more effective and less injurious extracorporeal method to fragment urinary stones [11]. Maxwell et al. [12] examined the feasibility of stone fracture by BWL applied to artificial and natural calculi in vitro. Also, they studied the characteristics of stone comminution by BWL.

Several researches have been done on ultrasonic lithotripsy. The waves' compression effects and cavitation phenomenon, are two important mechanisms on kidney stone fragmentation [13]. Wang [14] explained the effects of a bubble in the shock path to the elastic and fracture behaviors of the stone by using a multiphase fluid-solid coupled model. Maeda et al. [15, 16] experimentally and numerically studied cavitation when the BWL wave is used. They experimentally visualized bubble clouds using a high-speed camera. In addition, they applied a numerical method to model interactions among bubbles, stone and burst wave. Xi and Zhong [17] investigated the transient stress fields produced in stone of different geometries, sizes and general patterns of wave propagation using a dynamic photoelastic imaging technique. Dahake and Gracewski [18, 19] developed a linear elastic model of stress waves within the stone and studied the spherical and oval models of stone.
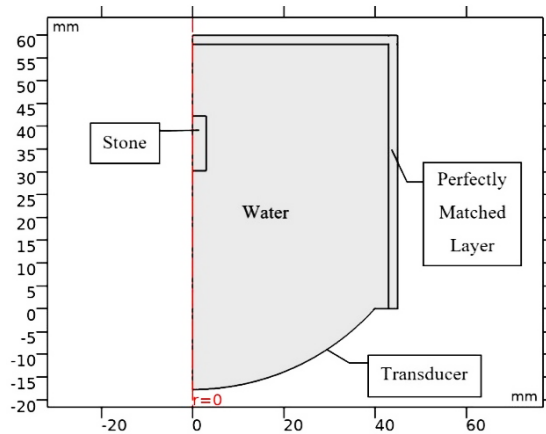
*Corresponding author's email: Shahidian@kntu.ac.ir

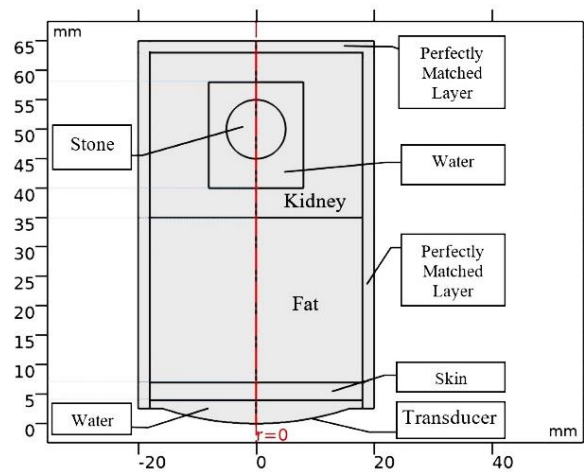**Fig. 1 Proposed model with a cylindrical stone for investigation of BWL**

Fig. 2. Proposed model of tissues and a spherical stone for investigation of synthesis of SWL and BWL

Cleveland and Sapozhnikov [20] applied a linear elasticity model based on the finite-difference method to fragmentation of kidney stones and to determine the location of maximum stress. Weinberg and Ortiz [21] numerically studied kidney damage and the fracture of kidney stone in extracorporeal shock wave lithotripsy. Moghimnezhad et al. [22] simulated the SWL method and its side effects using both linear and non-linear Westervelt equations. They demonstrated that applying the Westervelt equation leads to high accordance with reality. Ikeda et al. [23] applied a two-frequency ultrasound wave, a burst wave was used to generate cloud cavitation (bubble cloud) at the surface of the stone. Also, a second lower frequency wave was used to collapse the cloud to erode the stone.

Most numerical studies in lithotripsy have been carried out by using the elasticity method or energy method, which neglected the nonlinearity and dissipation of acoustic waves. In this research, the effects of ultrasonic waves on the stone and surrounding tissues are investigated by using the non-linear Westervelt equation. First, the effects of pressure amplitude, ultrasound frequency and stone's material for

BWL are investigated. Then, the combination of SWL and BWL are applied through the kidney and surrounding tissues model. Moreover, thermal analysis is carried out for both steps to indicate damages to surrounding tissue.

2- MATERIAL AND METHODS
2.1. Proposed Models
2.1.1.Burst Wave Lithotripsy
The schematic of the proposed model to investigate burst wave lithotripsy is depicted in Fig. 1, where stones are exposed to bursts wave for a duration of 10 cycles.

Aperture, focal length, axial beam width and lateral beam width of the transducer are 80 mm, 54 mm, 32.4 mm and 7.6 mm, respectively.

2.1.2.Synthesis of Burst and Shock Wave Lithotripsy
To consider the simultaneous effect of both methods (SWL and BWL) on stone fragmentation and surrounding tissues, the development of the geometry of Fig. 1 is required. Therefore, the schematic of the proposed model, kidney stone and surrounding tissues, is shown in Fig. 2.
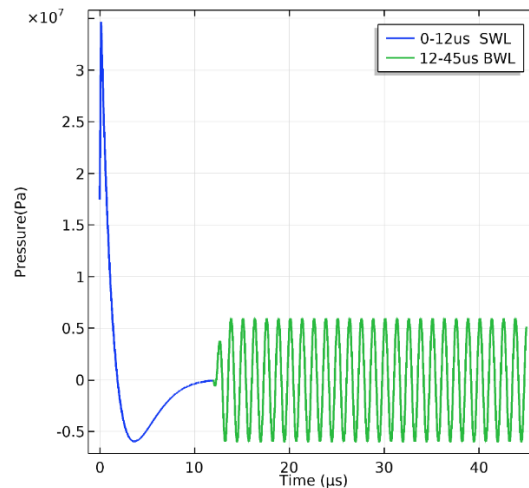
Fig. 3. Pressure profile of combined waves

Table 1. Materials' Properties [3, 26, 27-31]

Properties	Materials (Tissues and Stones)							
	Kidney	Fat	Skin	Water	COM	Uric acid	Struvite	Cystine
Speed of Sound (m/s)	1567	1476	1540	1520	4535	3471	2798	4651
Density (kg/m3)	1050	920	1190	1000	2038	1546	1587	1624
Nonlinearity Coefficient	7.4	10.28	7.87	5.2	7.4	7.4	7.4	7.4
Attenuation Coefficient (Np/m/MHz)	12	7	19.7	0.025	164	164	164	164
Specific Heat Capacity (J/Kg.c°)	3763	3221.7	3898	4180	1524	-	-	-
Thermal Conductivity (W/m.c°)	0.53	0.402	0.209	0.6	0.4	-	-	-
Young's modulus (GPa)	-	-	-	-	24.51	14.20	10.52	20.7
Poisson's ratio	-	-	-	-	0.333	0.39	0.24	0.37
Tensile Strength (MPa)	-	-	-	-	1.1	2.4	0.95	2.5

First, a shock wave with a maximum magnitude of 35 MPa is emitted for 12 microseconds to the tissues and stone. Then, a burst wave with a pressure amplitude of 6.5 MPa and a constant frequency of 800 kHz is radiated for 33 microseconds. The acoustic pressure inlet as a function of time is set to Eq.1 which is plotted in Fig. 3.

$$P(MPa) = \begin{cases} 2*35*\exp\left(-\dfrac{t}{1.96e-6}\right)* \\ \cos\left(\dfrac{t}{3.57e-6}+\dfrac{\pi}{3}\right) \ 0 < t < 12\,\mu s \\ 6.5*\sin\left(2*\pi*800e3*t+\dfrac{\pi}{3}\right) \\ 12 < t < 45\,\mu s \end{cases} \quad (1)$$

Surrounding tissues include skin, fat layer, kidney tissue and water are considered in the simulation. Space around the stone is filled with urine [24]. Because the urine is composed of 95% water [25], so water is considered as fluid around the stone.

The material of stone is assumed Calcium Oxalate Monohydrate (COM). In addition, Uric acid, Struvite and Cystine are studied. The properties of tissues and stones are provided in Table1.

2.2. Governing Equation

Investigation of lithotripsy and its thermal side effects on surrounding tissues is a Multiphysics problem and needs to couple acoustic pressure, elasticity and bio-heat transfer equations. The governing equations are as follows.

2.2.1. Acoustic Equation

The Westervelt equation which is a nonlinear full-wave equation is used to model acoustic field propagation in nonlinear thermoviscous fluids. The Westervelt partial differential equation is:

Table 2. The destructive thresholds of energy flux for biologic effects, due to pressure shock on the tissues [32, 33]

Biologic Effects	Energy Flux (mJ/mm^2)
The breakdown of endothelial cell structure	0.3
Changes in subcellular structures especially mitochondria	0.22
formation of tensile structure in the endothelium	0.1
Internal bleeding	0.045
Damage to skin	0.007

$$\nabla^2 p - \frac{1}{c^2}\frac{\partial^2 p}{\partial t^2} + \frac{\delta}{c^4}\frac{\partial^3 p}{\partial t^3} = -\frac{\beta}{\rho_0 c^4}\frac{\partial^2 p^2}{\partial t^2} \qquad (2)$$

Where p, c and ρ_0 are the acoustic pressure, speed of sound and the ambient density, respectively. Also δ and β are sound diffusivity of medium and the nonlinearity coefficient which are defined in equations 3 and 4 respectively.

$$\delta = 2\alpha \frac{c^3}{\omega^2} \qquad (3)$$

$$\beta = 1 + \frac{B}{2A} \qquad (4)$$

2.2.2. Elasticity Equation
The linear elasticity equation is applied.

$$\rho \frac{\partial^2 u}{\partial t^2} = \nabla . s + F_v \qquad (5)$$

Where u is displacement. F_v is external force, which is calculated and obtained by the acoustic equation.

2.2.3. Thermal Equation
The Pennes Bioheat equation is used to obtain the temperature distribution in tissues.

$$\rho_0 C_t \frac{\partial T}{\partial t} = \nabla k \nabla T + C_b w_b \left(T - T_b\right) + Q_{abs} \qquad (6)$$

In the Eq. 6, k, w_b, C_b, C_t and ρ are tissue thermal conductivity, the blood flow rate through the tissue, the blood specific heat capacity, tissue specific heat capacity and tissue density respectively. The perfusion time in the blood is in order of several thousand seconds and it can be neglected for a short period (several seconds).

Also, the Q_{abs} is heat source that is equivalent to the absorbed ultrasonic power in tissue. This heat source (acoustic intensity) is calculated by solving the acoustic equation in tissue.

$$Q_{abs} = 2\alpha_{abs}I = \alpha \frac{P^2}{\rho c} \qquad (7)$$

In Eq. 7, α, P and ρ are absorption coefficient, acoustic pressure and tissue density, respectively.

To determine the side effects of synthesis of SWL and BWL on kidney tissue, the acoustic intensity will be compared with the destructive thresholds of energy flux in the tissues, are given in Table 2.

2.2.4. Boundary Conditions
The pressure inlet is applied for the transducer boundary. Upper, right and left walls are considered as a perfectly matched layer. Background (initial) pressure within the entire domain is set to zero and the initial temperature is set to 37° c.

3- Numerical Procedure
COMSOL Multiphysics is used for numerical simulations. It is based on the finite element method for discretization and solution of the governing nonlinear transient differential equations in kidney stones and surrounding tissues. The nature of the problem requires the combination and coupling of acoustic wave propagation, the elasticity of structure and biological heat transfer equations. One-way coupling is employed to couple the acoustic and structural physics.

3.1. Grid Study
In acoustic simulations, considering the order of discretion, the number of meshes usually should be chosen at least 4 meshes per wavelength (λ). To achieve higher precision,
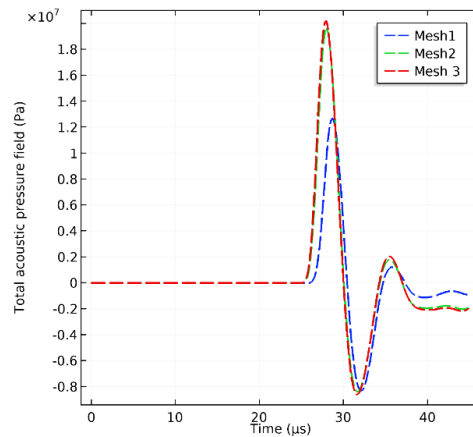
Fig. 4. Diagram of acoustic pressure versus time for three different meshes, which have 69958, 76887 and 83354 elements, respectively

Table 3. Mesh properties

Mesh	Number of meshes
1st	69958
2nd	76887
3rd	83354

the maximum mesh size is set to λ/6 with the fourth discrete order in the focal region and the places where the pressure gradient is higher (kidney and stones). In the other regions, the mesh size is set to λ/4 with the second discrete order. The number of meshes depends on the maximum wavelength of waves.

Mesh independency is studied by three different sizes of mesh. The triangular meshes are used, which the numbers of elements are given in Table 3. The pressure varieties at the front of stone versus time for different meshes are depicted in Fig. 4.

As shown in Fig. 4, the results illustrate the 2nd and 3rd meshes have a good match and the increase of mesh number from 76887 to 83354 does not change significantly the acoustic pressure profile. Therefore, the 2nd mesh is appropriate for the current simulation.

3.2. Verification

For verification purposes, our results are compared with the numerical simulation documented by Weinberg and Ortiz [21]. They measured the pressure through a domain under SWL with constant properties. Their proposed model is depicted in Fig. 5.

In our simulation, the shock wave is emitted in a homogeneous elastic medium with 1 MPa of Young's modulus and 1540 m/s of sound speed. The shock values are set to $\tau_1 = 1.1\,\mu s$, $\tau_2 = 1.96\,\mu s$, $P = 100\,MPa$ and the pressure profile is measured at 10 and 40 mm.

Wienberg and Ortiz [21] used the energy method and applied Eq. 8 to consider the dissipation parameter but we applied the Westervelt equation with $\beta = 4.7$, $\alpha = 12\dfrac{N_p}{m*MHz}$.

$$P_{damp} = \alpha_1 \rho c l_e \dot{\vartheta} \tag{8}$$

Where α_1 , ρ, c, l_e and $\dot{\vartheta}$ are the damping coefficient, density, the speed of sound, the longitudinal characteristic of the element and the volume traction rate.

The comparison of the current study and the Wienberg's results are presented in Fig. 6.

As depicted in Fig. 6, the overall trend and advent time of waves are similar. The difference of dissipation consideration leads to a slight difference in maximum pressure of the 40 mm data series between the current study and the Wienberg's results. At high pressures and frequencies, it is expected that the wave be deformed to a saw blade shape due to its nonlinearity. This point is clearly specified by the comparison of 40 mm and 10 mm series in our simulation. In contrast to this, it is not indicated in the Wienberg's results. Therefore, the results of the current study are more accurate.

4- RESULTS AND DISCUSSION

In the current study, two mechanisms of ultrasonic lithotripsy are investigated numerically. Burst wave lithotripsy and synthesis of SWL and BWL are studied on the stone and surrounding tissues. The Westervelt nonlinear equation is applied to model the acoustic waves. In addition, von Mises stress and temperature distribution are obtained by coupling and solving the governing equations. The results are presented in two separate sections: (l) Burst wave lithotripsy, and (2) Feasibility study of synthesis of shock and burst wave lithotripsy.
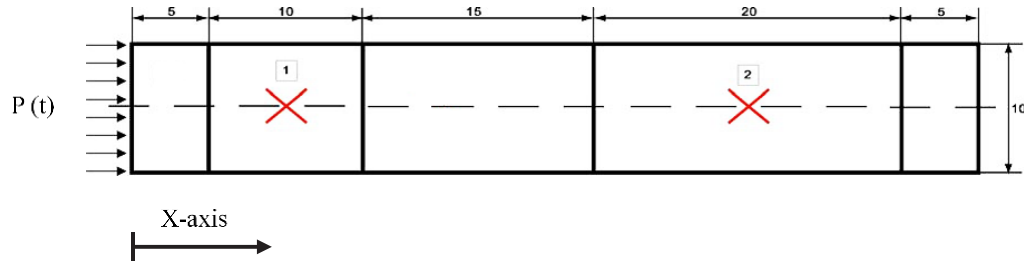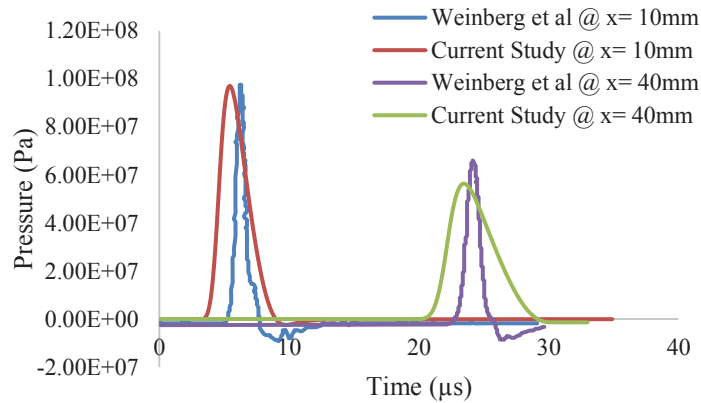
149

Fig. 5. The domain of Wienberg and Ortiz study [21]

Fig. 6. Comparison of impulses after 10 and 40 mm propagation for verification

4.1. Burst Wave Lithotripsy

4.1.1.Pressure Amplitude

Three burst waves with different pressure amplitudes of 1.2, 3 and 6.5 MPa at 170 kHz for COM stones are considered. Distribution of acoustic pressure and von Mises stresses for three different pressure amplitudes are depicted in Fig. 7.

As shown in Fig. 7, by increasing pressure amplitude, the position of focus remains constant, but the produced acoustic pressure and stress on the stone increase.

4.1.2.Ultrasound Frequency

In this section, the effect of ultrasound frequency variation on the distribution of acoustic pressure and von Mises stress is depicted in Fig. 8.

As shown in Fig. 8, the focal region is reduced by increasing the frequency. Therefore, an increase of frequency leads to a decrease in damages to adjacent tissues. At 170 kHz, the stress level of -6 dB appears at 3 mm inside the stone, and the pressure magnitude remains constant. At 285 and 800 kHz, the region with high stress is bigger. Therefore, the pieces of broken stones are smaller than stones at 170 kHz frequency. At 800 kHz, the average and maximum of produced von Mises stress are equal to 11 MPa and 103 MPa, respectively. At this frequency (800 kHz), because of the higher pressure than the tensile strength in the most parts of stone, it is expected that all parts of the stone are fragmented to small pieces, than the other frequencies. This point has a good agreement with the experimental outcome [12].

4.1.3.Stone Material

Von Mises stresses are obtained for four different stone materials. The pressure amplitude and ultrasound frequency are set to 6.5 MPa and 170 kHz, respectively. Distributions of von Mises stress are shown in Fig. 9.a. Furthermore, the ratio of maximum exerted von Mises stress to tensile strength for different stones are depicted in Fig. 9.b.

The stone will fragment if the von Mises stress becomes more than tensile strength. Not only is the amount of produced stress significant, but also the distribution of stress is effective in the fracture process. Distribution of stress depends on the stone's material and properties such as shape and size. Therefore, the material and geometry of stone have a key role to determine the optimum frequency of the BWL.

4.1.4.Thermal Analysis

Thermal analysis carried out on COM stone by applying the Pennes Bioheat equation, which is coupled with the Westervelt equation. The COM stone is exposed to bursts wave for a duration of 10 cycles with a frequency of 200 kHz. The temperature distribution is shown in Fig. 10.As depicted in Fig. 10, the temperature increases only inside the stone. Therefore, there is no thermal damage to surrounding tissues for the BWL.
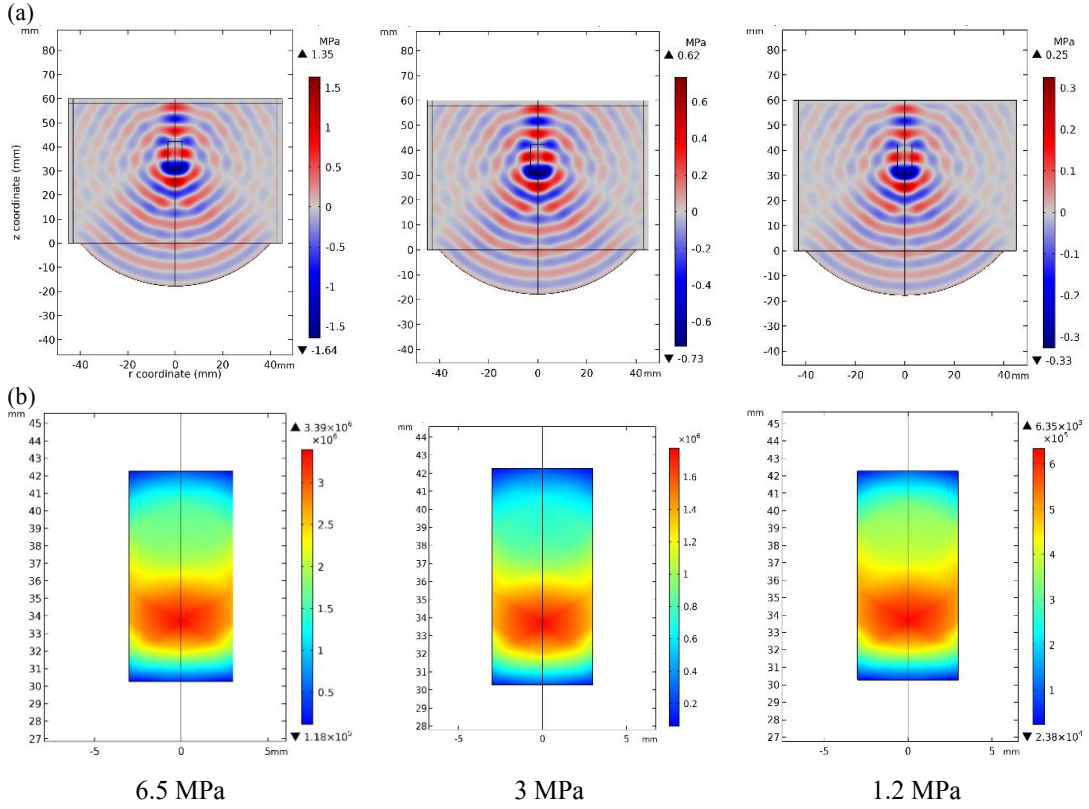
Fig. 7. Effect of focal pressure amplitude on COM stones (a) Distribution of acoustic pressure (b) Distribution of von Mises stresses
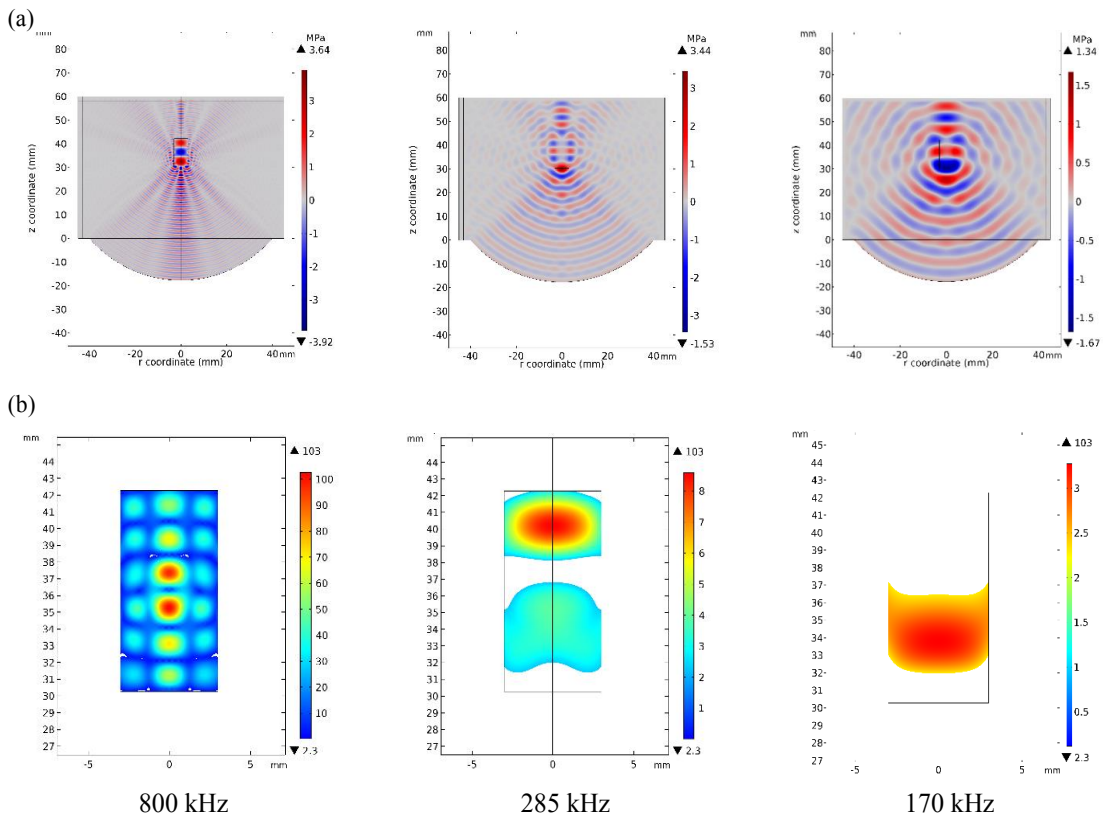

Fig. 8. Effect of ultrasound frequency on COM stones (a) Distribution of acoustic pressure (b) Distribution of von Mises stresses in the stones

(a)

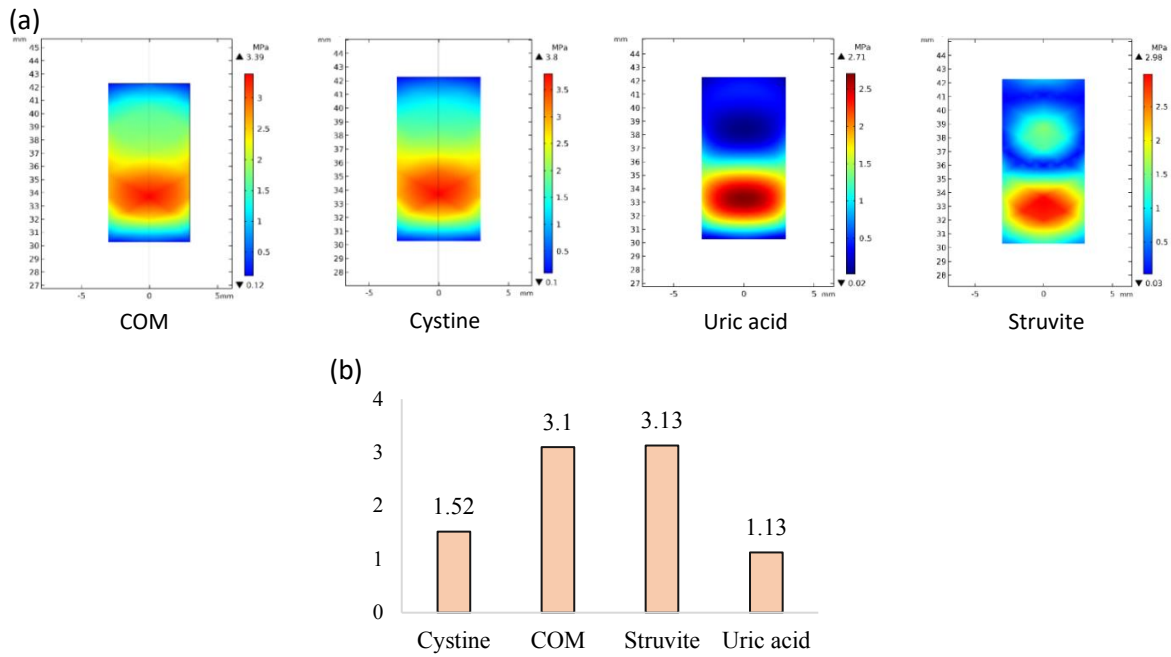COM   Cystine   Uric acid   Struvite

(b)

Fig. 9. Stress analysis on different material of stones (COM, Cystine, Uric acid and Struvite) (a) Distribution of von Mises stress (b) Ratio of maximum von Mises stress to tensile strength
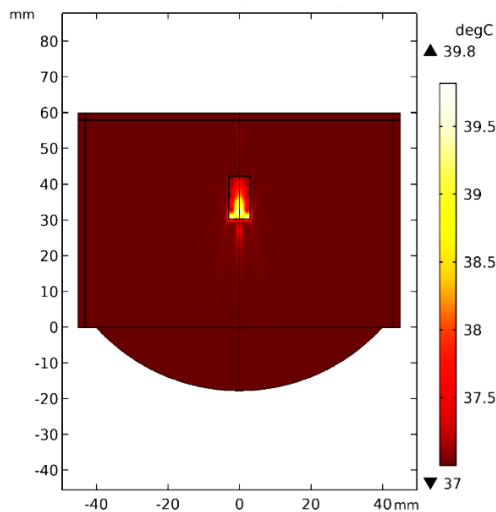

Fig. 10. Temperature distribution for BWL

4.2. Feasibility Study of Synthesis of Shock and Burst Wave Lithotripsy

In this section, the shock wave and burst wave are combined and utilized to investigate this method's feasibility. The distribution of pressure, acoustic intensity and temperature are obtained in the stone and surrounding tissues. First, a shock wave with a maximum magnitude of 35 MPa is emitted for 12 microseconds to the tissues and stone. Then, a burst wave with a pressure amplitude of 6.5 MPa and a constant frequency of 800 kHz is radiated for 33 microseconds (see Fig. 3).

Distribution of acoustic pressure for the synthesis of shock and burst waves is shown in Fig. 11.a. In addition, the pressure profile in the central axis ($r=0$) is depicted in Fig. 11.b. According to Fig. 11, the high-pressure region above the stone shows that the shock wave passed through the stone. Burst wave is conducted after the shock wave, due to the return of shock wave from the stone, a wall of a compressive wave is created at the front of the stone and prevents the burst wave to reach the stone. Therefore, the location of the maximum pressure is between 35 mm and 40 mm (kidney tissue) which indicated the increase of kidney tissue injury (Fig. 11.b). In order to prevent this effect, the burst wave should be emitted when the shock wave is damped, and it may take several microseconds.

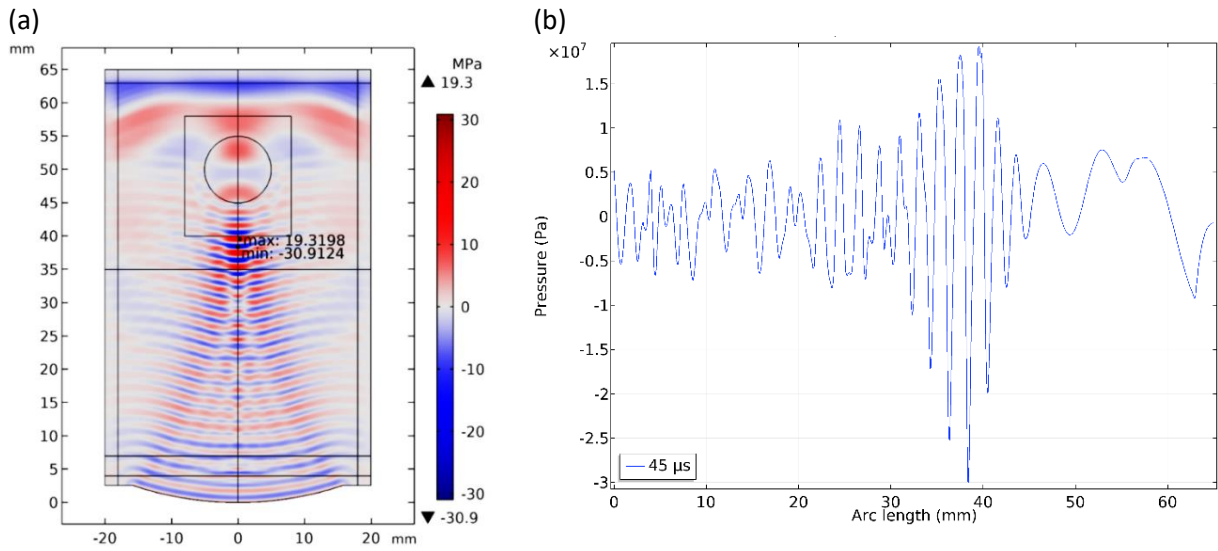Fig. 12 depicts the average of von Mises stress in the stone

(a)

(b)

Fig. 11. (a) Distribution of acoustic pressure in stone and surrounding tissues for the synthesis of shock and burst waves (b) Pressure profile in central axis (r=0)
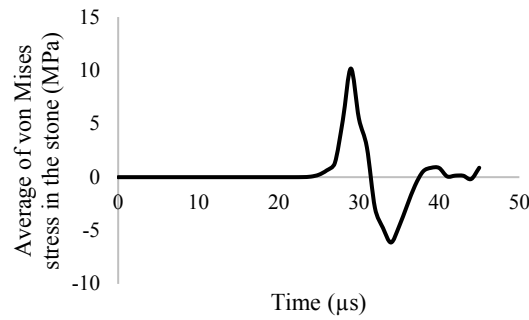
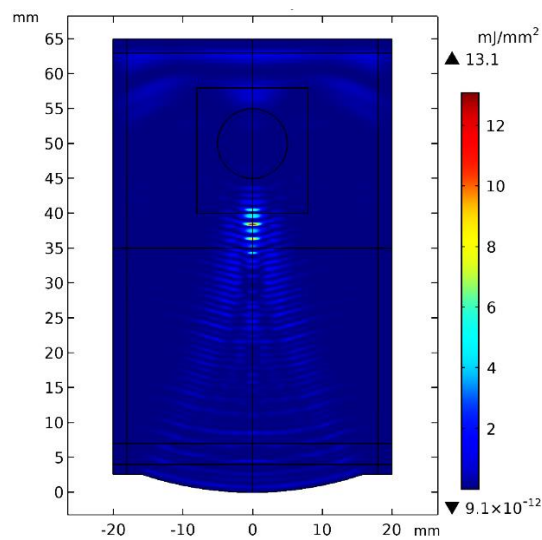**Fig. 12. Diagram of average von Mises stress in the stone vs. time**

Fig. 13 Distribution of acoustic intensity for the synthesis of SWL and BWL
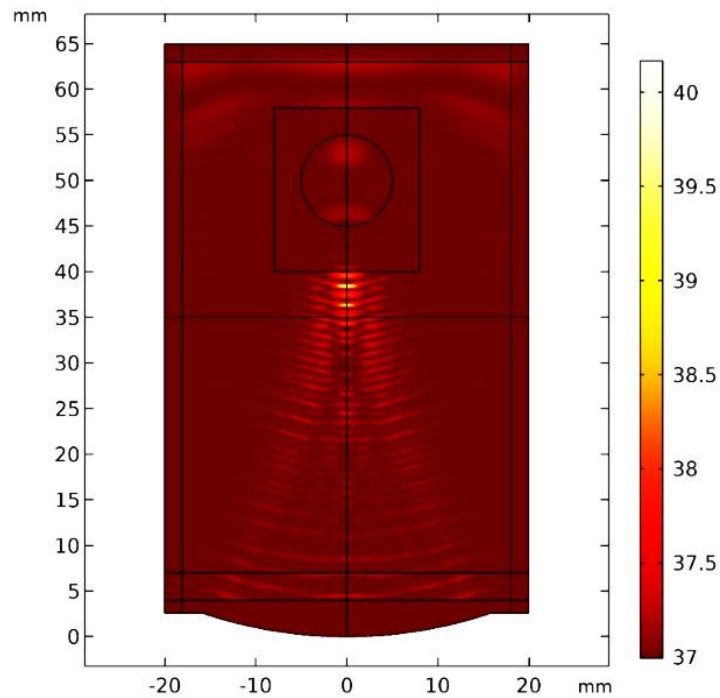
153

Fig. 14 Temperature distribution for the synthesis of SWL and BWL

versus time.

As shown, the shock wave reaches to stone and makes stress of 10 MPa at about 28μs. It is expected the burst wave appeared after spending 12 μs, but the average of von Mises stress converged into zero. This means that the burst wave cannot set up stress in the stone, because of the wall of the compressive wave which prevents the burst wave to reach the stone.

Distribution of acoustic intensity for the synthesis of SWL and BWL is depicted in Fig. 13.According to Fig. 13, the acoustic intensity is obtained about zero to 13.1 mJ/mm^2 in kidney tissue. Considering Table. 2, the destructive thresholds of energy flux on the tissues for injuries of cellular structure is 0.3 mJ/mm^2. Unfortunately, the synthesis of SWL and BWL has side effects on kidney tissues. So to prevent this effect, the burst wave should be emitted when the shock wave is damped, and it may take several microseconds.

In addition, the temperature distribution is obtained to illustrate more information about thermal injuries. The temperature contour is shown in Fig. 14.

As depicted, the temperature of kidney tissue rises 3°C. According to the results of Van Rhoon et al. [34], this increase causes primary damage to the kidney tissue.

5- CONCLUSION

In this study, the burst wave lithotripsy, synthesis of SWL and BWL, and their effects on surrounding tissues are investigated by coupling and solving the acoustic wave propagation, elasticity of structure and biological heat transfer equations.

To conclude, the following results are obtained.

Burst wave lithotripsy:

· By increasing pressure amplitude, the focus point remains constant, but the produced acoustic pressure and stress on the stone increase.

· By increasing ultrasound frequency the focal region is reduced. Therefore, an increase of frequency leads to a decrease in damages to adjacent tissues. At 800 kHz, because of the higher pressure than the tensile strength in most parts of stone, it is expected that all parts of the stone are fragmented to small pieces.

· By conducting stress analysis on four different materials of kidney stone, it is indicated that the stone's material has a key role in the distribution and amount of von Mises stress in the stones.

· Thermal analysis shows that the temperature increases only inside the stone. Therefore, there is no thermal damage to surrounding tissues for the burst wave lithotripsy.

Synthesis of SWL and BWL:

· Results show that the shock wave passed through the stone, and exerts stress in the stone. Then, due to the reflection of the shock wave from the stone, a wall of a compressive wave is created at the front of the stone and prevents the burst wave to reach the stone. Therefore, the burst wave cannot set up stress in the stone, and the location of the maximum pressure changes into kidney tissue.

· By comparing the acoustic intensity with destructive thresholds of energy flux, it is determined synthesis of SWL and BWL has side effects on kidney tissues. So to prevent this effect, the burst wave should be emitted when the shock wave is damped, and it may take several microseconds. In addition, the temperature of kidney tissue rises 3°C. This increase causes primary damage to the kidney tissue.

REFERENCES

[1] Aayani R, Shahidian A, Ghassemi M, Numerical Investigation of Non-Newtonian Blood Effect on Acoustic Streaming, J APPL FLUID MECH, 2016;9.

[2] Yousefi M, Pourmehran O, Gorji-Bandpy M, Inthavong K, Yeo L, Tu J. CFD simulation of aerosol delivery to a human lung via surface acoustic wave nebulization, Biomech Model Mechanobiol, 2017;16:2035-50.

[3] López-Haro S, Gutiérrez M, Vera A, Leija L, Modeling the thermo-acoustic effects of thermal-dependent speed of sound and acoustic absorption of biological tissues during focused ultrasound hyperthermia, J MED ULTRASON, 2015;42:489-98.

[4] Zohdi T, Krone R, Estimates for the acoustical stimulation and heating of multiphase biotissue, Biomech Model Mechanobiol, 2018;17:717-25.

[5] Mohammadalibeigi F, Shirani M, Seyed-Salehi H, Afzali L, Biochemical urinalysis of healthy kidney and stone-generating kidney in unilateral urolithiasis, J Renal Inj Prev, 2019;8.

[6] Zeng J, Wang S, Zhong L, Huang Z, Zeng Y, Zheng D, et al, A Retrospective Study of Kidney Stone Recurrence in Adults, J Clin Med Res, 2019;11:208.

[7] Eliahou R, Hidas G, Duvdevani M, Sosna J, Determination of renal stone composition with dual-energy computed tomography: an emerging application, Seminars in Ultrasound, CT and MRI: Elsevier, 2010. p. 315-20.

[8] Dai JC, Bailey MR, Sorensen MD, Harper JD, Innovations in Ultrasound Technology in the Management of Kidney Stones, Urologic Clinics, 2019.

[9] Wess OJ, Mayer J, Fragmentation of brittle material by shock wave lithotripsy, Momentum transfer and inertia: a novel view on fragmentation mechanisms, Urolithiasis, 2018:1-13.

[10] Lawler AC, Ghiraldi EM, Tong C, Friedlander JI, Extracorporeal shock wave therapy: current perspectives and future directions, Current urology reports, 2017;18:25.

[11] Zwaschka TA, Ahn JS, Cunitz BW, Bailey MR, Dunmire B, Sorensen MD, et al, Combined burst wave lithotripsy and ultrasonic propulsion for improved urinary stone fragmentation, Journal of endourology, 2018;32:344-9.

[12] Maxwell AD, Cunitz BW, Kreider W, Sapozhnikov OA, Hsi RS, Harper JD, et al, Fragmentation of urinary calculi in vitro by burst wave lithotripsy, J Urol, 2015;193:338-44.

[13] Ghorbani M, Oral O, Ekici S, Gozuacik D, Koşar A, Review on lithotripsy and cavitation in urinary stone therapy, IEEE reviews in biomedical engineering, 2016;9:264-83.

[14] Wang KG, Multiphase fluid-solid coupled analysis of shock-bubble-stone interaction in shockwave lithotripsy, INT J NUMER METH BIO, 2017;33:e2855.

[15] Maeda K, Colonius T, Kreider W, Maxwell A, Bailey M, Modeling and experimental analysis of acoustic cavitation bubble clouds for burst-wave lithotripsy, J Acoust Soc Am, 2016;140:3307-.

[16] Maeda K, Maxwell AD, Kreider W, Colonius T, Bailey MR, Investigation of the energy shielding of kidney stones by cavitation bubble clouds during burst wave lithotripsy, arXiv preprint arXiv:180106901. 2018.

[17] Xi X, Zhong P, Dynamic photoelastic study of the transient stress field in solids during shock wave lithotripsy, J Acoust Soc Am, 2001;109:1226-39.

[18] Dahake G, Gracewski S, Finite difference predictions of P-SV wave propagation inside submerged solids. II. Effect of geometry, J Acoust Soc Am, 1997;102:2138-45.

[19] Dahake G, Gracewski S, Finite difference predictions of P-SV wave propagation inside submerged solids. I. Liquid–solid interface conditions, J Acoust Soc Am, 1997;102:2125-37.

[20] Cleveland RO, Sapozhnikov OA, Modeling elastic wave propagation in kidney stones with application to shock wave lithotripsy, J Acoust Soc Am, 2005;118:2667-76.

[21] Weinberg K, Ortiz M, Kidney damage in extracorporeal shock wave lithotripsy: a numerical approach for different shock profiles, Biomech Model Mechanobiol, 2009;8:285.

[22] Moghimnezhad M, Shahidian A, Andayesh M, Multiphysics Analysis of Ultrasonic Shock Wave Lithotripsy and Side Effects on Surrounding Tissues, Journal of Biomedical Physics and Engineering, 2020.

[23] Ikeda T, Yoshizawa S, Koizumi N, Mitsuishi M, Matsumoto Y, Focused ultrasound and Lithotripsy, Therapeutic Ultrasound: Springer, 2016. p. 113-29.

[24] Bailey M, Khokhlova V, Sapozhnikov O, Kargl S, Crum L, Physical mechanisms of the therapeutic effect of ultrasound (a review), Acoustical Physics, 2003;49:369-88.

[25] Li W, Zhang J, Tse F, Handbook of LC-MS bioanalysis, New Jersey: Jonh Wiley and Sons, 2013.

[26] Ueberle F, Application of shock waves and pressure pulses in medicine, Springer Handbook of Medical Technology: Springer, 2011. p. 641-75.

[27] Warty Y, Haryanto F, Fitri LA, Haekal M, Herman H, A Spatial Distribution Analysis on the Deposition Mechanism Complexity of the Organic Material of Kidney Stone, Journal of Biomedical Physics and Engineering, 2019.

[28] Haddadi S, Ahmadian MT, Numerical and Experimental Evaluation of High-Intensity Focused Ultrasound–Induced Lesions in Liver Tissue Ex Vivo, J Ultrasound Med, 2018;37:1481-91.

[29] Suomi V, Jaros J, Treeby B, Cleveland RO, Full modeling of high-intensity focused ultrasound and thermal heating in the kidney using realistic patient models, IEEE Transactions on Biomedical Engineering, 2018;65:969-79.

[30] Kyriakou A, Multi-physics computational modeling of focused ultrasound therapies: ETH Zurich, 2015.

[31] Nyame YA, De S, Sarkissian C, Brown R, Kartha G, Babbar P, et al, Kidney stone models for in vitro lithotripsy research: A comprehensive review, Journal of endourology, 2015;29:1106-9.

[32] Steinbach P, Wörle K, Seidl M, Seitz R, Hofstädter F, Effekte hochenergetischer Ultraschallstoßwellen auf Tumorzellen in vitro und humane Endothelzellen.

Stoßwellenlithotripsie, Aspekte und Prognosen Attempt Tübingen S, 1995:104-9.

[33] Miller DL, Thomas RM, Thresholds for hemorrhages in mouse skin and intestine induced by lithotripter shock waves, Ultrasound Med Biol, 1995;21:249-57.

[34] Van Rhoon GC, Samaras T, Yarmolenko PS, Dewhirst MW, Neufeld E, Kuster N, CEM43° C thermal dose thresholds: a potential guide for magnetic resonance radiofrequency exposure levels? European radiology, 2013;23:2215-27.